Supporting Information

Differentiating and Quantifying Gas-Phase Conformational Isomers Using Coulomb Explosion Imaging

Shashank Pathak[1], Razib Obaid[2,#], Surjendu Bhattacharyya[1], Johannes Bürger[3], Xiang Li[1], Jan Tross[1,##], Travis Severt[1], Brandin Davis[2], René C. Bilodeau[2,4], Carlos Trallero[2], Artem Rudenko[1], Nora Berrah[2], and Daniel Rolles[1]

[1]*J.R. Macdonald Laboratory, Department of Physics, Kansas State University, Manhattan, KS, USA*
[2]*Department of Physics, University of Connecticut, Storrs, CT, USA*
[3]*Department of Physics, Ludwig Maximilian University of Munich, Germany*
[4]*Advanced Light Source, Lawrence Berkeley National Laboratory, Berkeley, CA*
[#]*Current address - RARAF, Columbia University, Irvington, NY, USA.*
[##]*Current address – Sandia National Lab*

1) Experimental details and momentum reconstruction

The VMI spectrometer and detector assembly (microchannel plate detector with delay-line anodes, RoentDek DLD80 for the electrons and RoentDek HEX80 for the ions) used in our experiment is shown in Figure S1. The setup is different from a conventional VMI apparatus in that we can record the time of flight as well as the impact positions of each ion and electron in coincidence using delay-line anodes. The experimental apparatus is identical to the one used in previous studies[1-3], where the setup and data analysis are discussed in detail, and both are hence only briefly described here. The spectrometer consists of a set of extractor plates, focusing lenses, and drift tubes on both sides of interaction region in order to guide ions and electrons to their respective detector by an inhomogeneous constant electric field. For this study, the voltages applied were +210 V and -210V to the two inner-most extractor/repeller electrodes, +1080 and -1260 V to the focusing lenses, and +5980 V and -5600 V to the two drift tubes. With these voltages, it was possible to collect electrons up to 300 eV and singly charged ions up to 25 eV, over the full solid angle. In the ALS multi-bunch mode, the time interval (2 ns) between the soft X-ray pulses is too short to unambiguously assign photoelectrons, Auger electrons, and fragment ions to a specific soft X-ray pulse. The time of flight of the ionic fragments (shown in Figure S2) is thus measured with respect to the arrival time of the first electron detected in coincidence.

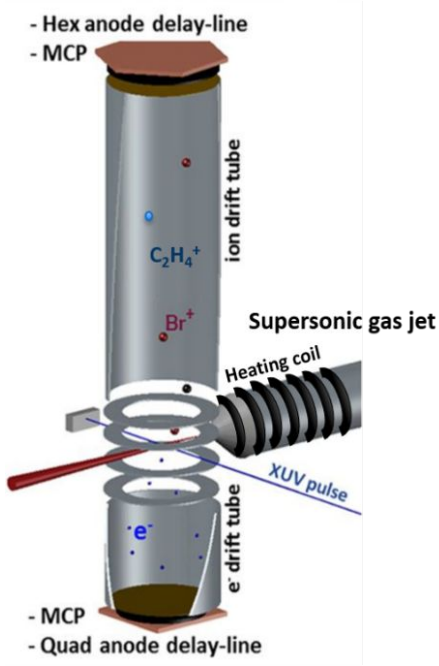

Figure S1: Schematic of the experimenal setup. It consists of a double-sided VMI spectrometer[3] equipped with time and position sensitive delay line detectors on each side for measuring ions and electrons in coincidence. Also shown is the supersonic molecular beam source with heating coil to heat the nozzle and sample line for temperature-dependent studies.

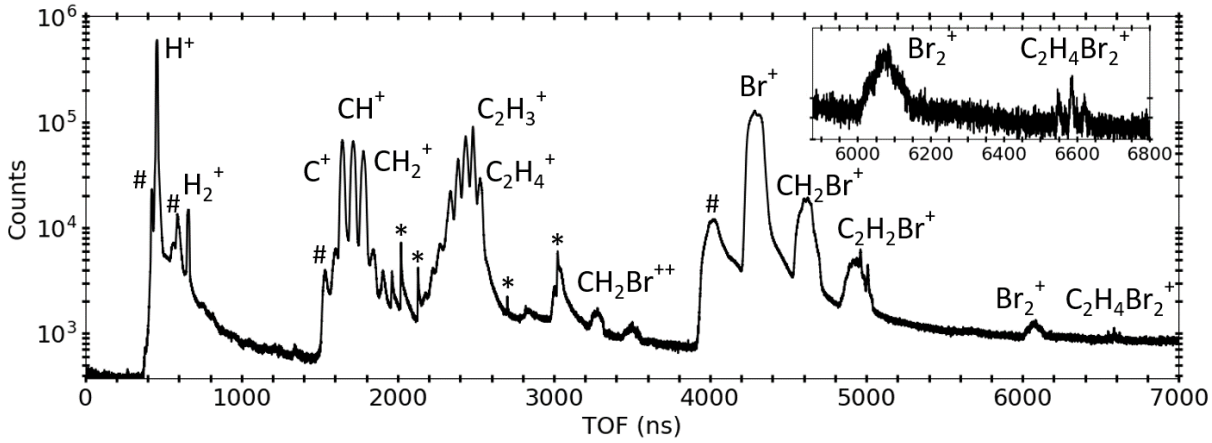

Figure S2: Ion time-of-flight spectrum of 1,2-dibromoethane recorded after photoionization at 140 eV photon energy. The inset shows a zoomed-in view of the spectral region including singly charged molecular bromine and the singly ionized parent, 1,2-dibromoethane. Peaks from background residual gas are marked with '*'. The peaks marked with '#' are from secondary electrons created by ion impact on the mesh that terminates the drift tube. These electrons are accelerated towards the MCP, where they are detected at slightly shorter flight times than the corresponding ions.

In other words, the signal from the electron microchannel plate detector is used as a trigger and start signal for recording the time of flight of the ionic fragments, while no time-of-flight information is recorded for the electrons. Hence, we only record the 2-dimentional projection of the total momentum for electrons (from the position signals), which can be converted to 3-dimentional momentum distribution using standard VMI inversion techniques[4]. On the other hand, both the hit position and time-of-flight information for the ionic fragments are recorded for each fragment, which are then used to calculate the full 3-dimensional momenta for all ionic fragments produced by the X-ray pulse. As the electric field in a VMI is inhomogeneous in the spatial dimensions, there is no analytical formula to calculate the initial velocities (and momenta) for the ionic fragments based on their time of flight and hit position. Instead, we simulate the hit position and time of flight for different velocities for a given ionic fragment using the SIMION 8.1 software[5]. Using these simulations, we can then calculate the three-dimensional momenta and kinetic energies for each ion recorded in coincidence[3].

1,2-dibromoethane or EDB (purity >99%) was purchased commercially from Sigma Aldrich. EDB is liquid at room temperature and has a vapor pressure of 11.7 mmHg (at 25 °C). It was filled in a bubbler (~10-15 ml), degassed using several freeze-pump-thaw cycles, and inserted into the experimental chamber, which is under ultra-high vacuum, using a supersonic expansion through a flat-aperture nozzle of 30 μm in diameter. The vapor pressure of EDB was high enough to introduce it in the chamber without using carrier gas. For recording data at different sample temperature, the entire sample delivery system was heated, including the sample reservoir and the sample delivery line, which were set to a few degrees lower temperature than the nozzle temperature to achieve a positive temperature gradient from reservoir to nozzle in order to avoid sample condensation. The whole assembly was thermalized before recording data for each

temperature; hence, the equilibrium sample temperature before the supersonic expansion is expected to be very close to the nozzle temperature.

Figure S2 shows the time-of-flight (TOF) mass spectrum of EDB after ionization at 140 eV photon energy. The spectrum displays many peaks, indicating rich fragmentation into various ionic species along several pathways. The parent ion (EDB^+) has 3 peaks (Figure S2, inset) due to the two stable isotopes of Br, ^{79}Br and ^{81}Br, with natural abundances of 50.7 % and 49.3 %, respectively. The yield of EDB^+ is relatively low compared to those of fragments ion such as CH^+, $C_2H_3^+$ and Br^+ since the singly charged parent ion is almost exclusively produced by valence ionization, which has a low cross section at this photon energy. We do not observe peaks in the TOF spectrum corresponding to the parent dication (EDB^{2+}) or trication (EDB^{3+}), suggesting that those are unstable and dissociate into several fragments on a timescale faster than the typical flight times of a few microseconds. The triple ion coincidence channel $C_2H_4^+ + Br^+ + Br^+$ (with any combination of isotopes), which we chose for the further analysis, represents ~13% of the total triple ion coincidence yield, and the $C_2H_4^+ + {}^{81}Br^+ + {}^{81}Br^+$ coincidence channel contains a quarter of those events.

2) Subtraction of sequential events using the native frames method

One of the main ideas of the native frames method[6] is to analyze each fragmentation step in its respective center-of-mass (c.o.m.) frame, i.e. its native frame. This is accomplished by using the conjugate momenta derived from Jacobi coordinates associated with each fragmentation step. To be specific, for a sequential breakup of type $ABC^{3+} \rightarrow AB^{2+} + C^+$ as a first step, and $AB^{2+} \rightarrow A^+ + B^+$ as second step, the first step is analyzed in the c.o.m. frame of ABC^{3+}, and second step is analyzed in the c.o.m. frame of AB^{2+}. If the intermediate fragment AB^{2+} rotates with a lifetime longer than its rotation period and in the final fragmentation plane, a uniform distribution of the angle $\theta_{AB,C}$ is expected, where $\theta_{AB,C}$ is the relative direction of the unimolecular dissociation of AB^{2+} with respect to the emission direction of C^+ (as shown in Figure S3). In Figure S3, the red arrow represent the second step breakup and the black arrow represents first step breakup. From the analysis in the native frames, we can also calculate the kinetic energy release (KER) of the second step, denoted by KER_{AB}. KER_{AB} frequently helps in identifying metastable states of the intermediate fragment[6]. The second step KER (KER_{AB}) is defined as

$$KER_{AB} = \frac{p_{AB}^2}{2\mu_{AB}}$$

where p_{AB}^2 is the relative momentum and μ_{AB} is the reduced mass of A^+ and B^+ fragments. In the next step, all 3-body fragmentation events in the channel $A^+ + B^+ + C^+$ are plotted as a function of KER_{AB} and $\theta_{AB,C}$. In this plot, the sequential fragmentation proceeding through the AB^{2+} as intermediate can be clearly identified as a uniform angular distribution in the angle $\theta_{AB,C}$. This process is then repeated for different intermediate fragments (e.g. BC^{2+} or AC^{2+}) to identify events corresponding to a sequential breakup with those intermediates.

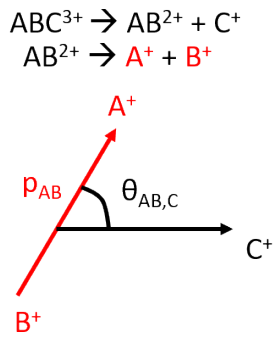

Figure S3: Representation of the relative angle and momenta for a typical 3-body sequential breakup. The black arrow and red arrow represent the first and second step, respectively.

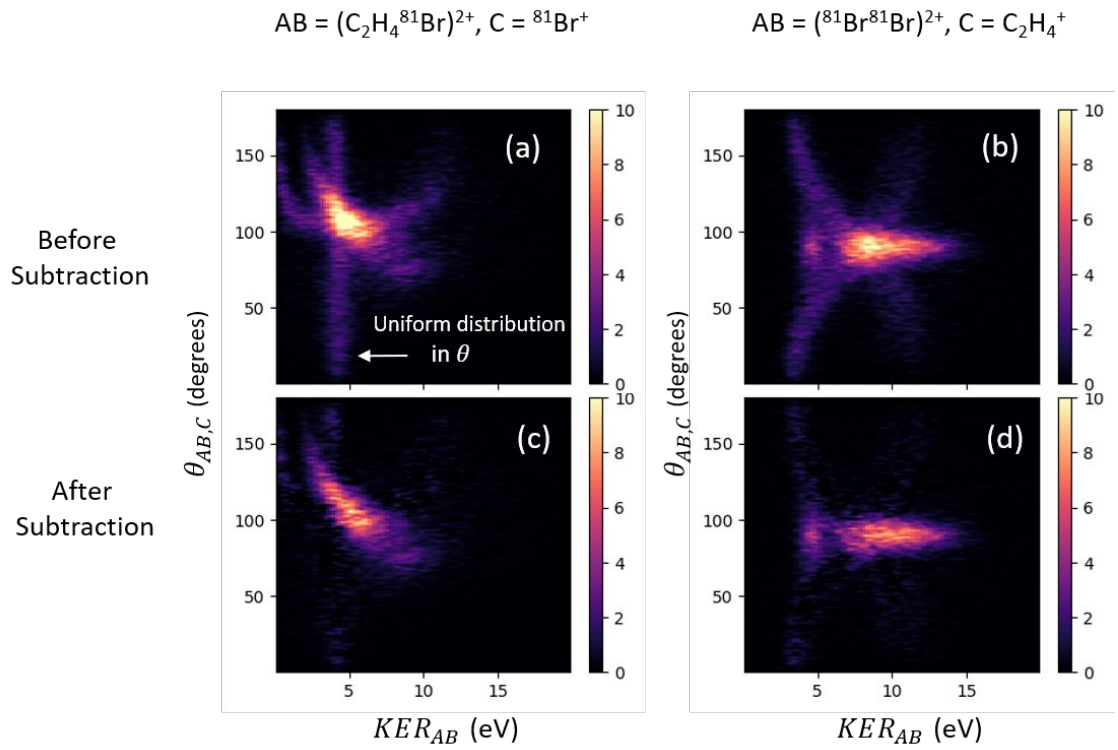

Figure S4: For a sequential breakup of type $ABC^{3+} \rightarrow AB^{2+} + C^{+}$ in the first step and $AB^{2+} \rightarrow A^{+} + B^{+}$ in the second step, all 3-body fragmentation events in the channel $A^{+} + B^{+} + C^{+}$ can be plotted as a function of KER_{AB} and $\theta_{AB,C}$, where KER_{AB} is the KER of second step and $\theta_{AB,C}$ is the angle between the relative momenta of fragments formed in each step of the *sequential* breakup. The sequential events with AB as intermediate appear as being uniformly distributed over all angles (see text). (a), (b) shows each event in the 3-body coincidence channel $C_2H_4^{+} + {}^{81}Br^{+} + {}^{81}Br^{+}$, plotted as a function of KER_{AB} and $\theta_{AB,C}$ for two different choices of AB: (a) $AB \equiv (C_2H_4{}^{81}Br)^{2+}$, $C \equiv {}^{81}Br^{+}$; (b) $AB \equiv ({}^{81}Br{}^{81}Br)^{2+}$, $C \equiv C_2H_4^{+}$. The white arrow in panel (a) points to the uniform distribution in angle, suggesting sequential fragmentation via this pathway, while no such signature of a uniform distribution in angle is visible in (b). Panel (c),(d) show the data from panels (a),(b) after subtracting the contribution from sequential fragmentation.

Here we summarize our results of the native frames analysis for the case of the $C_2H_4^+ + {}^{81}Br^+ + {}^{81}Br^+$ 3-body fragmentation channel in 1,2-dibromoethane. Figure S4 shows all 3-body fragmentation events in the $C_2H_4^+ + {}^{81}Br^+ + {}^{81}Br^+$ breakup channel, plotted as a function of KER_{AB} and $\theta_{AB,C,}$ where AB^{2+} and C^+ are the ions formed in the first step of sequential fragmentation. Figure S4(a) shows the plot for the intermediate $AB \equiv (C_2H_4{}^{81}Br)^{2+}$ and $C \equiv {}^{81}Br^+$. The uniform distribution in angle $\theta_{AB,C}$ can be clearly seen (highlighted by the white arrow), which corresponds to the sequential events with the intermediate $(C_2H_4{}^{81}Br)^{2+}$. Other features in this plot correspond to concerted breakup and to sequential breakup processes via different intermediates. Figure S4(b) shows the same data plotted for the intermediate $AB = ({}^{81}Br{}^{81}Br)^{2+}$ and $C = C_2H_4^+$. One can easily conclude given the geometry of the molecule that the intermediate chosen in this case is very unlikely to be the intermediate in a sequential breakup since the two bromine atoms are not directly bonded to each other. As expected, the plot does not show a uniform distribution over all angles, indicating no contribution from sequential fragmentation with a $({}^{81}Br{}^{81}Br)^{2+}$ intermediate. Nevertheless, Figure S4(b) is useful for separating the contributions from *anti* and *gauche* concerted breakup events, which can be seen as two clearly separate spots in this representation and each of which can thus be easily selected using a rectangular region-of-interest (ROI).

Before gating on these two regions, we can, in addition, subtract the sequential breakup events, which allows us to retrieve the concerted breakup yield for *anti* and *gauche* conformers. In order to retrieve the concerted breakup events, the native frames method exploits the uniform distribution of events over $\theta_{AB,C}$ in the KER_{AB} vs $\theta_{AB,C,}$ plot: First, we choose only that part of the data in Fig. S4(a) where the events from the sequential breakup are clearly separated from the other contributions (in this case, we chose the range of $\theta_{AB,C,} = [10,30]$). Additional events for the remaining $\theta_{AB,C}$ range are then generated by duplicating the data from the chosen range and randomly assigning a value for $\theta_{AB,C}$ to each event. We thus generate a uniform distribution of events in $\theta_{AB,C}$ while preserving the statistical fluctuations in the data. This generated data is then subtracted from the distribution of events in Fig. S4(a) in order to separate out the distribution of concerted events in the region where they strongly overlap with sequential events. Figures S4(c) and (d) show the resulting plots after subtracting the sequential breakup events from panels S4(a) and (b). Some of the weak structures which appear after subtraction are due to the "leftover" sequential events which are not statistically significant, which is verified by integrating the yield around the weaker structures.

The concerted breakup distributions can also be plotted as Newton plots to verify the procedure. Figures S5(a) and (b) show the resulting Newton plots containing only the sequential events (generated using the native frames method) with ${}^{81}Br^+$ emitted in first step and the $(C_2H_4{}^{81}Br)^{2+}$ intermediate breaking up as a second step for $C_2H_4^+ + {}^{81}Br^+ + {}^{81}Br^+$ breakup channel. As mentioned previously, the semi-circular ring in Figure S5(a) is a signature of the intermediate fragment $(C_2H_4{}^{81}Br)^{2+}$ rotating with respect to the ${}^{81}Br^+$ fragment (represented by the black arrow), which is emitted in the first step of the sequential breakup. The difference between Figure S5(a) and Figure S5(b) is that the former is plotted using those ${}^{81}Br^+$ as reference ions that are emitted in the first step of the sequential breakup (as identified by the native frames method), while the latter is plotted with those ${}^{81}Br^+$ as a reference that are emitted in second step of

sequential breakup. Figure S5(c) shows only the "concerted" events, after subtracting the "sequential" events generated using the native frames method. Figure S5(d) shows all events in the $C_2H_4^+ + {}^{81}Br^+ + {}^{81}Br^+$ breakup channel for comparison, which clearly includes all three of the above contributions.

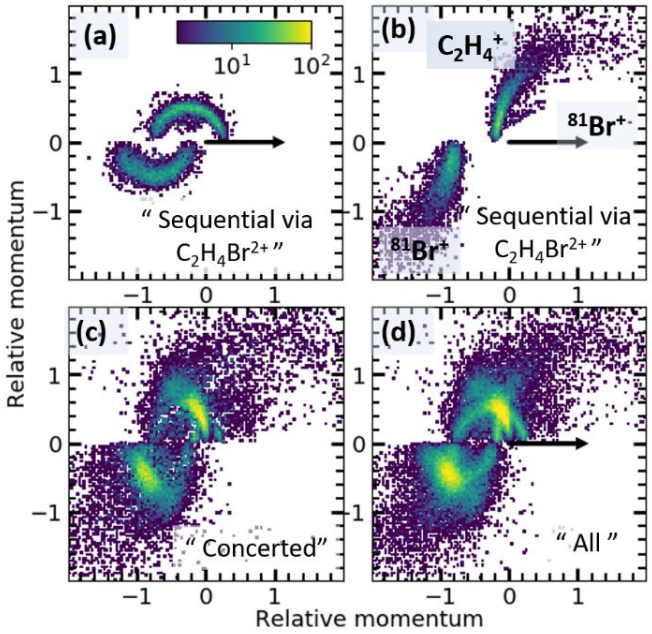

Figure S5: Newton plots showing the normalized relative momenta of each fragment in the 3-body coincidence channel $C_2H_4^+ + {}^{81}Br^+ + {}^{81}Br^+$, with one of the $^{81}Br^+$ fragments chosen as the reference ion plotted along the X axis, the $C_2H_4^+$ fragment in upper half of the plot, and the other $^{81}Br^+$ fragment in the lower half. (a) Sequential breakup channel with $(C_2H_4{}^{81}Br)^{2+}$ as an intermediate. The events are generated via the native frames method (see text). (b) Sequential breakup channel with $(C_2H_4{}^{81}Br)^{2+}$ as an intermediate, plotted for the incorrect breakup sequence. (c) Concerted breakup channel, obtained by subtracting the events in panel (a) and (b) from all events (shown again in panel (d) for comparison).

3) Coulomb explosion simulation (CES) for the concerted breakup channel $C_2H_4^+ + Br^+ + Br^+$

The equilibrium geometries of *gauche* and *anti* conformers, shown in Figure S6, are determined using the open source package Avogadro[7]. Classical CES are performed considering three point charges – one at the position of each of the two bromine atoms, and the third charge at the center-of-mass (c.o.m.) of C_2H_4. In order to account for small geometry changes of the molecule, e.g., because of vibrations in the neutral or ionic states, either due to the initial temperature of the sample or due to vibrational excitation during the ionization process, we randomly vary the position of both bromine atoms within a sphere around their equilibrium position. For the simulations shown in Figure 3 and 4 of the main text, the radius of this sphere is chosen to be 5% of the C-Br bond distance. We generate 1000 such randomly sampled pairs of bromine

coordinates, and determine the coordinate of third point charge (at the c.o.m. of C_2H_4 moiety) such that the c.o.m. of the distorted molecule remains exactly the same as in the equilibrium geometry since the c.o.m. of the molecule does not move during vibrations along the normal modes of the molecule. It is to be noted that for each geometry, we consider the molecule to be at rest and neglect the velocity that any atom might posses due to vibrational motion. For each distribution of three point charges, the classical equations of motions under the influence of Coulomb repulsion are then solved using a standard ordinary differential equation solver to determine the trajectories and hence the asymptotic velocity/momentum of each charged fragment. Figure S7 shows the distribution of charges for *gauche* and *anti* geometries for which the simulations were performed. The positions of the charges on the bromine atoms are shown in red, and the position of the charge at the center-of-mass of the C_2H_4 is shown in blue. The solid black dots show the position of the bromine atoms and the c.o.m. of C_2H_4 for the equilibrium geometry.

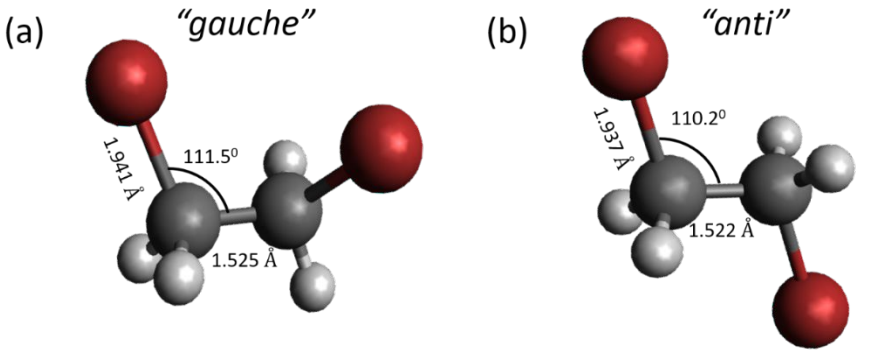

Figure S6: Equilibrium geometries of (a) *gauche* and (b) *anti* conformers of EDB computed using Avogadro[7].

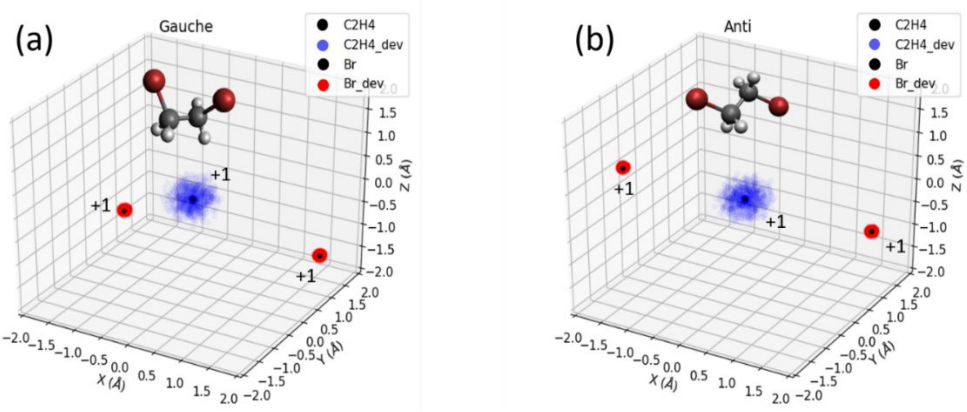

Figure S7: Distribution of point charges for 1000 randomly generated near-equilibrium geometries of (a) *gauche* and (b) *anti* conformers for which the Coulomb explosion simulations were performed (see text). The solid black dots show the equilibrium positions for the two bromine atoms as well as c.o.m. of the

C_2H_4. The red and blue dots show the deviation (from the equilibrium position) of bromine atoms and c.o.m. of C_2H_4 respectively, as chosen for the simulation.

References

1. Ablikim, U.; Bomme, C.; Xiong, H.; Savelyev, E.; Obaid, R.; Kaderiya, B.; Augustin, S.; Schnorr, K.; Dumitriu, I.; Osipov, T.; et al. Identification of absolute geometries of cis and trans molecular isomers by Coulomb Explosion Imaging. *Sci. Rep.* **2016,** *6*, 38202.

2. Ablikim, U.; Bomme, C.; Savelyev, E.; Xiong, H.; Kushawaha, R.; Boll, R.; Amini, K.; Osipov, T.; Kilcoyne, D.; Rudenko, A.; et al. Isomer-dependent fragmentation dynamics of inner-shell photoionized difluoroiodobenzene. *Phys. Chem. Chem. Phys.* **2017,** *19*, 13419-13431.

3. Ablikim, U.; Bomme, C.; Osipov, T.; Xiong, H.; Obaid, R.; Bilodeau, R. C.; Kling, N. G.; Dumitriu, I.; Augustin, S.; Pathak, S.; et al. A coincidence velocity map imaging spectrometer for ions and high-energy electrons to study inner-shell photoionization of gas-phase molecules. *Rev. Sci. Instruments* **2019,** *90*, 055103.

4. Gascooke, J. R.; Gibson, S. T.; Lawrance, W. D. A "circularisation" method to repair deformations and determine the centre of velocity map images. *J. Chem. Phys.* **2017,** *147*, 013924.

5. SIMION. version 8.1, The field and particle trajectory simulator, Scientific Instrument Services, Inc (2013). http://simion.com/.

6. Rajput, J.; Severt, T.; Berry, B.; Jochim, B.; Feizollah, P.; Kaderiya, B.; Zohrabi, M.; Ablikim, U.; Ziaee, F.; Raju P, K.; et al. Native Frames: Disentangling Sequential from Concerted Three-Body Fragmentation. *Phys. Rev. Lett.* **2018,** *120*, 103001.

7. Hanwell, M. D.; Curtis, D. E.; Lonie, D. C.; Vandermeersch, T.; Zurek, E.; Hutchison, G. R. Avogadro: An advanced semantic chemical editor, visualization, and analysis platform. *J. Cheminformatics* **2012,** *4*, 17.